# The Dependence of Regioregular Poly(3-hexylthiophene) Film Morphology and Field-Effect Mobility on Molecular Weight

*R. Joseph Kline,[1] Michael D. McGehee,[1]\* Ekaterina N. Kadnikova,[2] Jinsong Liu,[2] Jean M. J. Fréchet [2,3] and Michael F. Toney[4]*

[1]Department of Materials Science & Engineering, Stanford University, Stanford, CA 94305

[2]Department of Chemistry, University of California, Berkeley, CA 94720

[3]Materials Science Division, E.O. Lawrence Berkeley National Laboratory, Berkeley, CA 94720

[4]Stanford Synchrotron Radiation Laboratory, Menlo Park, CA 94025

\* Electronic Mail: mmcgehee@stanford.edu

**Abstract**

Morphological characterization has been used to explain the previously observed strong correlation between charge carrier mobility measured with thin-film transistors and the number-average molecular weight (MW) of the conjugated polymer regioregular poly(3-hexylthiophene). Atomic force microscopy and x-ray diffraction show that the low mobility, low MW films have a highly ordered structure composed of nanorods and the high mobility, high MW films have a less ordered, isotropic nodule structure. Modifying the morphology for a constant MW by changing the casting conditions or annealing the samples strongly affects the charge transport and morphology in the low mobility, low MW films, but has little effect on the high MW films. In-plane grazing incidence x-ray scattering shows the in-plane $\pi$-stacking peak increases when the mobility increases for a constant MW. When the MW is changed, this correlation breaks down, confirming that in-plane $\pi$-stacking does not cause the mobility-MW relationship. We believe a combination of disordered domain boundaries and inherent effects of chain length on the electronic structure cause the mobility-MW relationship.

**Keywords:**

## Introduction

Conjugated polymers have been developed into very useful materials for a variety of applications, including light emitting diodes,[1,2] photovoltaic cells (PVs)[3-5] and thin-film transistors (TFTs).[6-8] The operation of polymer PVs and TFTs are limited by the charge carrier mobility of the polymer. Therefore, understanding the determining factors of the mobility is key to improving the performance of polymer PV and TFTs. High mobility polymer TFTs (mobility of 0.01-0.1 cm$^2$/Vs) have been made with poly(-9,9' dioctyl-fluorene-co-bithiophene) (F8T2),[9,10] poly[5,5'-bis(3-dodecyl-2-thienyl)-2,2'-bithiophene] (PQT)[11,12] and regioregular poly(3-hexylthiophene) (P3HT).[13-17] The charge carrier mobility of P3HT has been related to regioregularity,[18] number-average molecular weight (MW),[19,20] casting solvent,[13,21] and carrier concentration.[22] The properties of polyfluorene films also depend on MW.[23,24] The present work shows how MW, casting solvent, and processing conditions affect the charge carrier mobility of P3HT TFTs.

We have previously shown that varying the MW of P3HT by one order of magnitude results in a four orders of magnitude change in the field-effect charge carrier mobility in TFTs[19] and a factor of 15 increase in the mobility of space-charge-limited current (SCLC) diodes of P3HT.[25] The low mobility, low-MW films have a highly ordered structure consisting of nanorods, whereas the high mobility, high-MW films have an isotropic nodule structure. We hypothesized that the domain boundaries in the low-MW films and the shorter chain length caused the mobility to be low in these films. These results were obtained from unannealed films cast from chloroform onto substrates treated with hexamethyldisilizane (HMDS). Neher et al have confirmed these results, but explained the mobility-MW relationship with a model, in which low MW films have highly ordered crystallites in an amorphous matrix with the mobility limited by

the amorphous regions.[20] Neher et al propose that the low-MW molecules tend to adopt a twisted, disordered conformation similar to that previously observed in higher molecular weight films at elevated temperatures.[26] We now provide further experimental evidence to support our original model and show that the observations of Neher et al also support our model. Others have shown that the amount of in-plane π-stacking is correlated with the mobility dependence on solvent[21] and regioregularity.[18] We will show in this paper that in-plane π-stacking cannot explain the mobility dependence on MW.

**Experimental**

To test the hypotheses about the cause of the mobility difference, steps have been taken to modify the morphology, while keeping the MW constant. The morphology was modified by annealing the film, changing the casting solvent[27] and changing the casting conditions. The polymers were classified as low ($M_{n,GPC}$ < 4 kD), medium ($M_{n,GPC}$ ~ 10 kD) and high-MW ($M_{n,GPC}$ > 30 kD). The polymers and electrodes used were fabricated as described previously.[19] All polymers reported in this study are synthesized by the modified McCullough route using 2-methylthiophene as an end-capping agent[28] and have regioregularities greater than 98% as measured by ^{1}H NMR. MW was adjusted by controlling the ratio of 2-methylthiophene to the monomer. The details of the polymers are reported elsewhere.[19] All processing and electrical testing was completed in a nitrogen-purged glove box. Substrates were cleaned in a UV ozone cleaner and then treated with HMDS by spin casting from a 20:80 solution of HMDS : propylene glycol monomethyl ether acetate at 4500 RPM. Spin-casting of the P3HT was done at at 2000 RPM from concentrations of 2-5 mg/ml in chloroform unless noted otherwise. Solutions were heated to 60 $^o$C for 30 minutes to dissolve the polymer before spin coating. The resulting films

were typically 20-50 nm thick. The annealed samples were spin cast from chloroform, heated for 1 hour at 125 $^{\circ}$C in an inert atmosphere and allowed to slowly cool to room temperature over 30 minutes. Drop-cast films were cast from a dilute chloroform solution (0.5 mg/ml) and were enclosed in a Petri dish to increase the evaporation time to about 30 minutes. Reported mobilities were measured in the saturation regime by taking the slope of the square root of the drain current plotted against the gate voltage and fitted to the saturation regime equation.[29]

$$\mathbf{I_{ds}} = \frac{\mathbf{W}}{\mathbf{2L}} \mathbf{C_i} \, \mu \, \left(\mathbf{V_g} - \mathbf{V_t}\right)^2 \mathbf{V_d} \qquad\qquad (1)$$

Atomic force microscopy (AFM) and x-ray diffraction (XRD) samples were deposited onto substrates similar to those used for TFTs but without the gold electrodes, while absorption samples were deposited onto similarly treated glass substrates. A Veeco multimode AFM using Nanodevices TAP150 AFM probes was used to make the AFM measurements in tapping mode in air. The nanorods were only resolvable with very sharp tips. Polymer molecules easily adsorbed to the tip and typically reduced the resolution (within one or two scans) to the point at which the nanorods were no longer resolvable. For this reason fresh tips were used for each sample.  A Phillips Expert x-ray diffractometer was used to measure the out-of-plane diffraction with copper $K_\alpha$ x-rays. Stanford Synchrotron Radiation Laboratory beam line 7-2 was used in grazing incidence geometry with a beam energy of 9 keV to measure in-plane diffraction. Samples were tested in a helium ambient to prevent the beam from damaging the sample. Repeated scans showed no evidence of damage. The incident angle was 0.2 degrees and the scattered beam resolution was 1 mrad. Absorption measurements were made with an Ocean Optics UV-Vis spectrometer.

**Results**

Figure 1 shows the results of annealing, casting from a higher boiling point solvent (xylene), and drop-casting on the charge carrier mobility of TFTs. The low-MW films are more strongly affected by these processes than the high-MW films are. Each of these processes increases the low-MW mobility by a factor of 50-100; whereas the mobility of the high-MW films increases by less than a factor of 5. The overall trend of increasing mobility with increasing MW is still observed, although the effect is reduced to a factor of 100 from the previous factor of 10,000. This suggests that at least part of the mobility difference in un-annealed spin cast films is due to
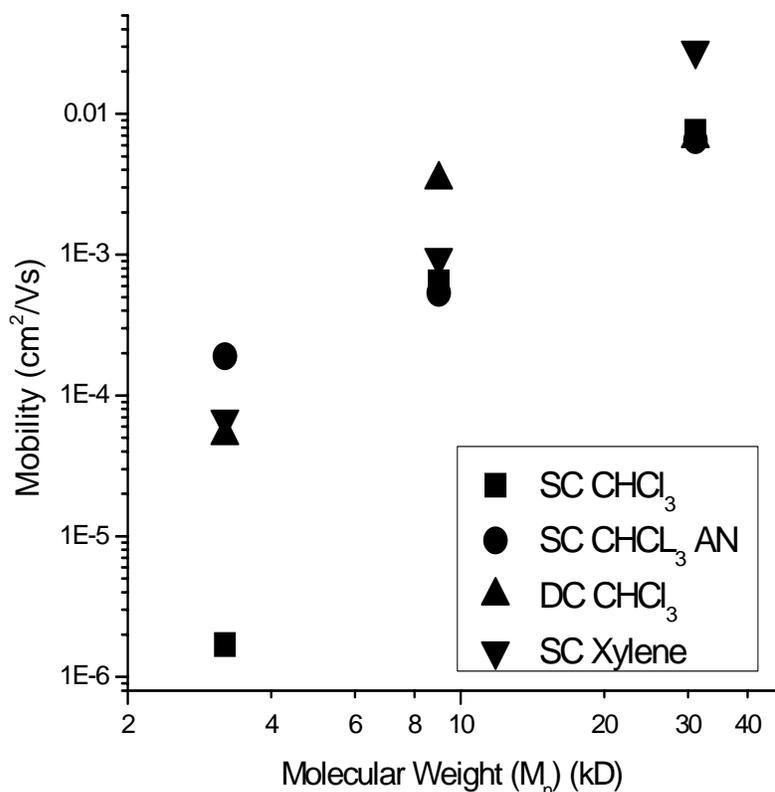


**Figure 1** – Comparison of change in charge carrier mobility for three different MWs as the processing conditions are changed. Samples are spin-cast (SC) from chloroform, annealed (AN), drop-cast (DC), or spin-cast from xylene.

the morphology and is not inherent to the effects of chain length on charge transport.

AFM images of the low-MW chloroform-cast, xylene-cast and annealed chloroform-cast films show substantial differences in morphology (figure 2). The AFM images show that the nanorods are clearly resolved in both the topography and phase signals across the entire area of the scan. Dark areas in the phase images, such as the ones highlighted with a circle, correspond to depressions in the film and not disordered areas, suggesting that there are no surface regions where the molecules are amorphous. The nanorods in the xylene-cast, the annealed chloroform-
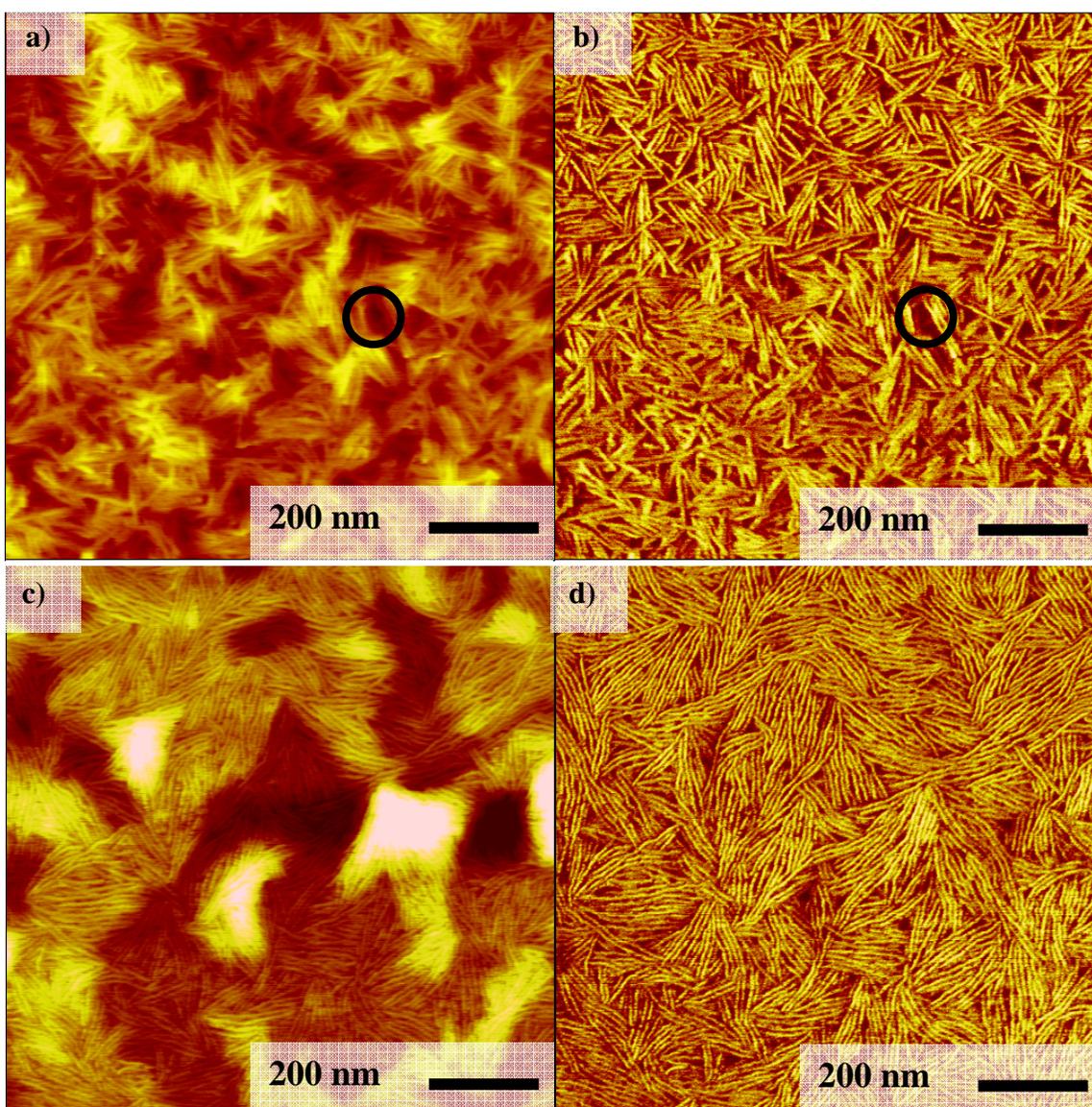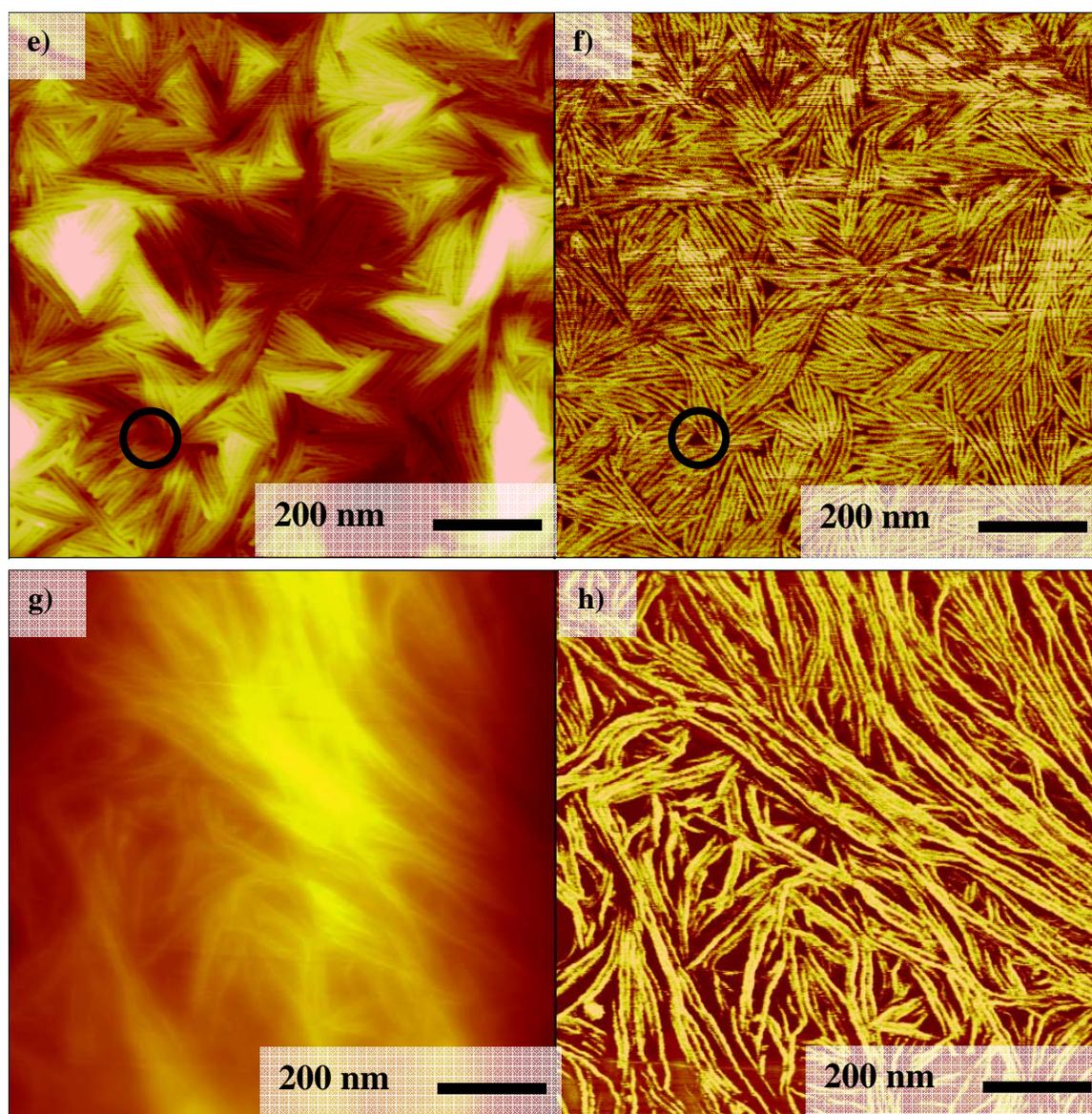
**Figure 2** – Atomic Force Microscope images comparing low-MW films spin-cast from chloroform [a) topography and b) phase], xylene [c) topography and d) phase], annealed after spinning from chloroform [e) topography and f) phase] and drop-cast from chloroform [g) topography and h) phase]. Circles denote a dark area in the phase image and the corresponding areas in the topography. Z-range is 10 nm except in drop-cast film where it is 100 nm.

cast and the drop-cast films are locally ordered and appear to be better connected with neighbors, whereas the nanorods in the chloroform-cast film appear loosely connected and randomly oriented. The nanorods in the xylene-cast, the annealed chloroform-cast and the drop-cast films are also much longer than those of the chloroform-cast film. The better connectivity of neighboring rods would be expected to make inter-rod transport easier by increasing the electronic overlap between neighboring nanorods, and could explain the increased mobility if transport in low-MW films is limited by the boundaries between the nanorods. Additionally the increased length of the nanorods should reduce the number of required inter-rod hops to traverse the film. Little difference was observed in AFM images of the different high-MW films for each of the processes. All of the high-MW films appear to have an isotropic nodule-like structure.[19]

   Out-of-plane XRD spectra comparing the low and high-MW chloroform films to the xylene films show both xylene films to have substantially higher crystallinity than their chloroform counterparts (figure 3). This would be expected since the higher boiling point of xylene should allow the spin cast films more time to reach their equilibrium structure during film formation. This effect was recently observed to be stronger with an even higher boiling point solvent, trichlorobenzene, for high-MW films.[21] Similar results should be obtained from spin-casting a chloroform film in a solvent-saturated environment. All films are also crystallographically textured, with preferential ordering of the alkyl spacing direction (100) normal to the substrate. These observations are in agreement with what has been previously shown.[18] Out-of-plane XRD of the annealed and drop cast low-MW films show no noticeable differences in peak intensity from the low-MW chloroform film, but have sharper peaks.

   Since the charge carriers in TFTs are confined to a thin layer adjacent to the semiconductor-gate dielectric interface, the out-of-plane diffraction is only indirectly related to the TFT charge
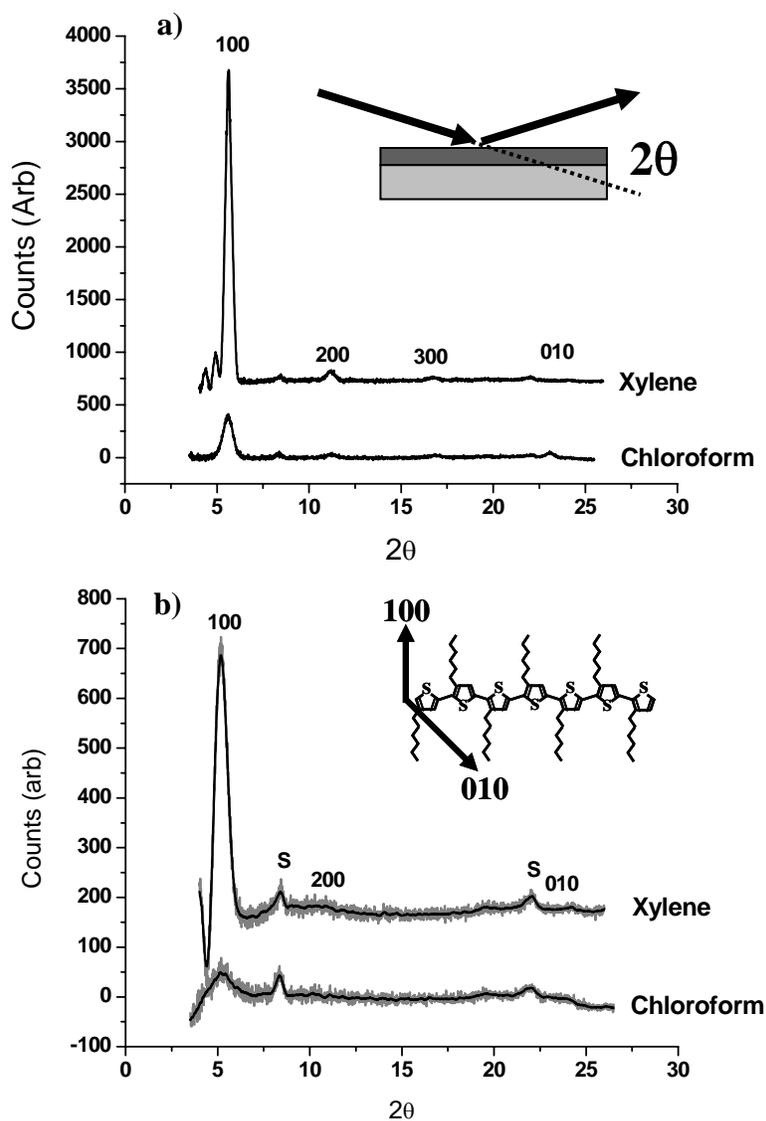
**Figure 3** – Out-of-plane x-ray diffraction comparing low (a) and high (b) MW films spin-cast from chloroform and xylene. Inset in a) shows the geometry of the diffraction experiment and the inset in b) shows the molecule and scattering directions. Substrate peaks are marked with **s**.

transport. To directly measure the pertinent ordering, grazing incidence x-ray scattering (GIXS) from a synchrotron source was used. GIXS is strongly surface-sensitive since the electric field intensity of the x-rays decays exponentially with depth into the sample. The grazing angle can be adjusted to determine the penetration depth and limit scattering from the substrate. Silicon oxide

in the underlying substrate has a very broad scattering peak that overlaps with the π-stacking peak of P3HT. This peak was minimized by using a shallow grazing angle and a substrate with a thin-oxide layer. GIXS has been previously used to determine the change in morphology in P3HT associated with regioregularity,[18] dip-coating[30] and solvent.[21,31]

GIXS data for low and high-MW films from each of the processing conditions are compared in figure 4. The GIXS data is plotted in terms of the scattering vector (q), which is related to the scattering angle in equation 2. Surprisingly, the spectra show ordering for both the alkyl chain

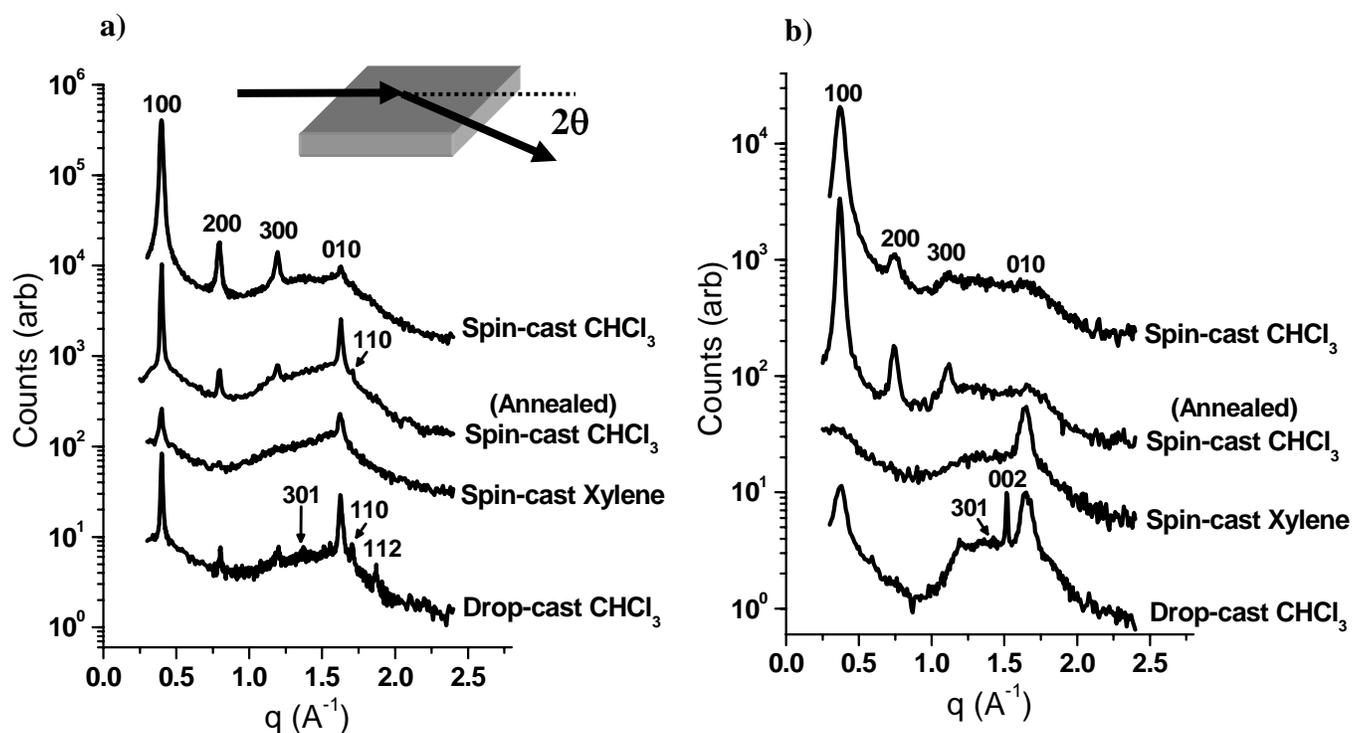$$q = \frac{4\pi}{\lambda} \sin \theta \qquad (2)$$



**Figure 4** – In-plane grazing incidence XRD data for low (a) and high-MW (b) films processed by spin-casting from chloroform (before and after anneal), spin-casting from xylene and drop-casting from chloroform. The π-stacking peak (010) increases for the xylene and drop cast films.

direction (100) and the π-stacking (010) in-plane. The intensity of the π-stacking peak increases with each of the processing conditions at constant MW when the charge carrier mobility increases, and stays about the same in the high-MW annealing case where the mobility decreases slightly. This relationship between the in-plane π-stacking peak and the mobility has been previously observed.[18] The drop cast films show mixed index peaks in-plane, indicating the presence of two and three-dimensional ordering with very little crystallographic texturing.

Comparisons of GIXS data for high and low-MW films with identical processing conditions show that the low-MW films have much sharper peaks than the high-MW films (figure 5). The peak width is determined by the crystal size and/or the variations in spacing within a crystal.[32] It
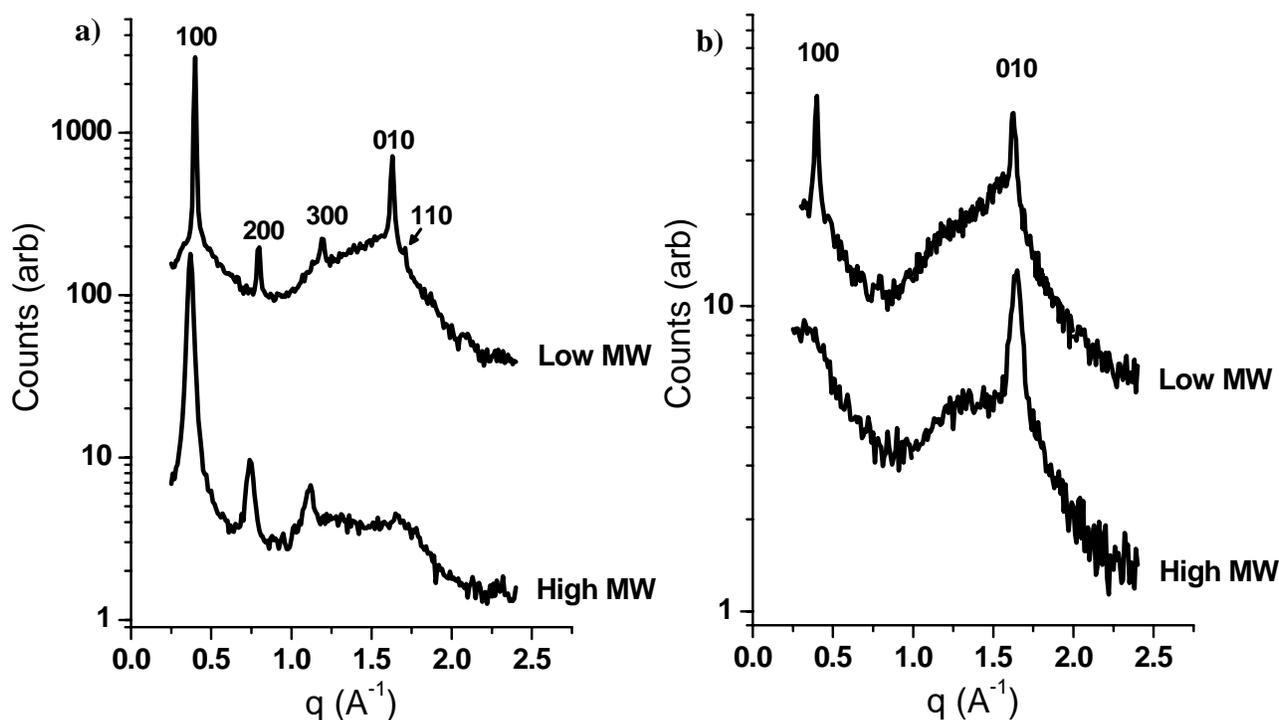


**Figure 5** – In-plane grazing incidence XRD data comparing low-MW films to high-MW films with varying processing condition. a) compares annealed high and low-MW films spin cast from chloroform and b) compares high and low-MW films spin cast from xylene.

seems likely that the low-MW films would have both larger crystals and less variation in d-spacing. The annealed samples (figure 5a) show a case where the film with a substantially larger π-stacking peak has a mobility 80 times lower. This strongly suggests that in-plane π-stacking is not the primary reason for the mobility difference between high and low-MW films. The xylene spin-cast samples (figure 5b) show a case with slight differences in the amount of in-plane π-stacking with MW, but a mobility difference of 300.

**Discussion**

AFM and XRD measurements show clear morphological differences between the low and high-MW films. The low-MW films have well-defined nanorods that are much larger than the ordered domains of the high-MW films. One might expect that this increased order would provide better charge transport, but this is not the case. A proposed chain-packing model is shown in figure 6 to help explain this observation. The low-MW polymer molecules are only about 8 nm long, so they are expected to behave like rigid rods. Figure 6a suggests that the molecules in a nanorod are highly ordered along the nanorod axis, but that the orientational order between the nanorods is low. We hypothesize that the nanorods in the low-MW film are poorly connected and that charge transport between nanorods is consequently hindered. This hypothesis is supported by the increase in mobility observed in the annealed, drop-cast and xylene spin-cast low-MW films. AFM characterization of these films shows local ordering of the nanorods that suggests improved inter-rod overlap. Since GIXS shows that the in-plane π-stacking also increases, it is difficult to conclusively determine the relative importance of these two effects on mobility.
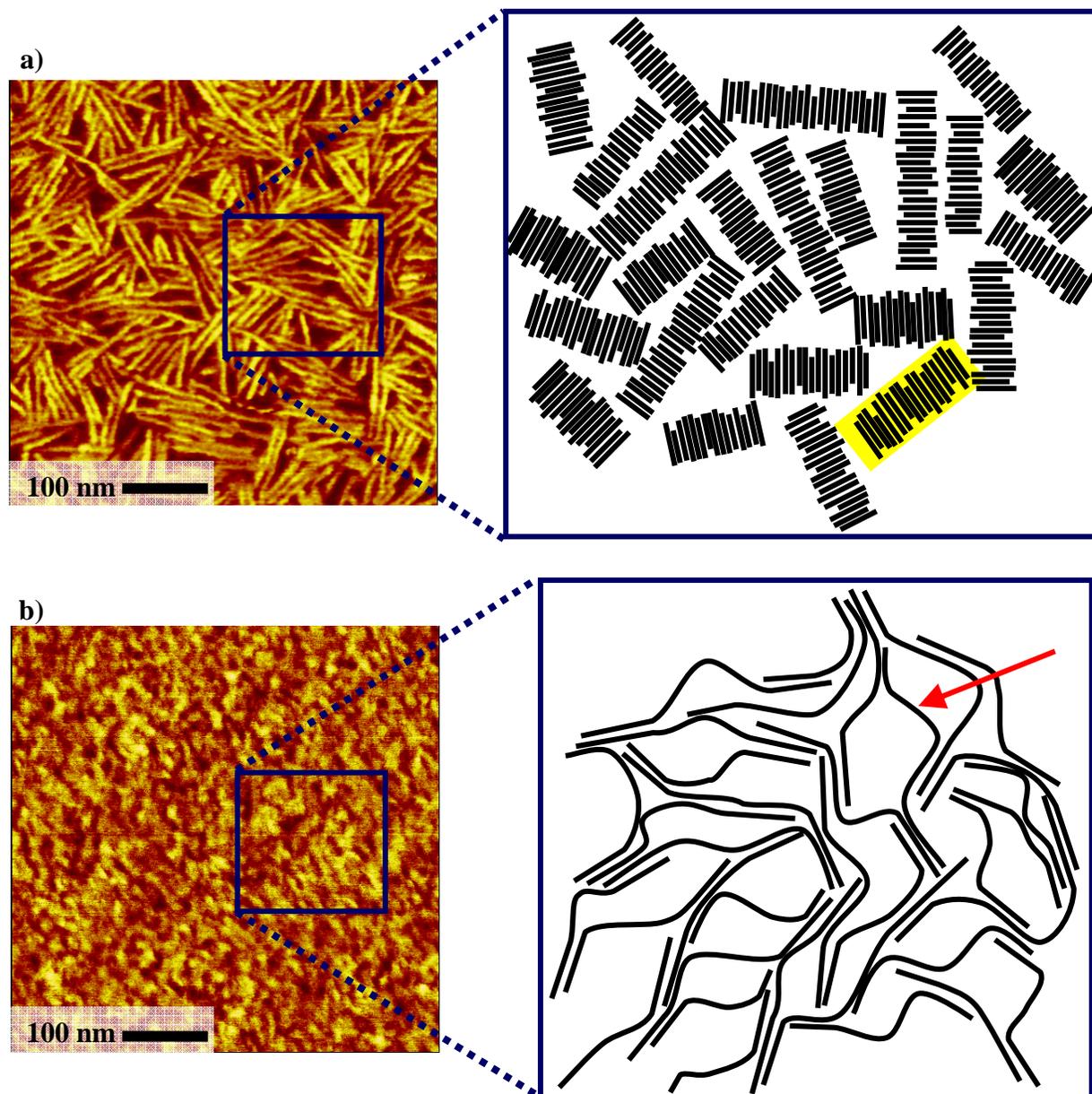
**Figure 6 –** Model for transport in low (a) and high-MW (b) films. Charge carriers are trapped on nanorods (highlighted in yellow) in the low MW case. Long chains in high-MW films bridge the ordered regions and soften the boundaries (marked with arrow).

AFM images show that the width of the nanorods is constant across the film, independent of processing conditions and similar to the length of the low-MW polymer chains (8 nm). This suggests that the molecules lie with their chain axis in the plane of the substrate and

perpendicular to the long axis of the nanorods (figure 6a). Out-of-plane diffraction shows strong alkyl chain stacking normal to the substrate, and thus normal to the nanorods, suggesting that the π-stacking direction is along the long axis of the nanorod. AFM images of low-MW nanorod monolayers show step heights of multiples of 1.6 nm, corresponding to the alkyl chain spacing, further supporting this model for molecular orientation. The AFM images (figure 2) show a film that appears to be highly ordered, with very little room for disordered areas that could have their alkyl chain axis in the plane of the substrate. Since AFM only measures the surface structure of the 20-nm thick film, another phase could be present in the bulk of the film to account for the alkyl chain diffraction observed in the in-plane measurements.

The persistence length of regiorandom P3HT has been reported to be 2.1 nm,[33] but since the regioregularity defects cause twists in the polymer chain, the persistence length of highly regioregular P3HT should be significantly longer. The high-MW polymer molecules are about 80-nm long. Since this is almost certainly longer than the persistence length, the molecules are expected to have multiple bends along their length. We hypothesize that the high-MW molecules form small ordered areas separated by disordered regions (figure 6b). We propose that the long chains can interconnect ordered areas and prevent charge carriers from being trapped by the disordered boundary regions by creating a continuous pathway through the film. The increase in mobility observed in high MW films when drop-casting from chloroform and changing the spin-casting solvent from chloroform to xylene corresponds to an increased in-plane π-stacking. The xylene case shows that the highest mobility occurs when no in-plane alkyl chain stacking is observed (figure 4b). This observation is in agreement with the results of others.[18] Interestingly, while the in-plane and out-of-plane diffraction for the xylene case is substantially different from the chloroform spin cast case, the mobility difference is only a factor of 5 for high-MW.

Evidence that the mobility-MW relationship is not primarily due to the in-plane $\pi$-stacking is shown in figure 5a. Large differences in in-plane $\pi$-stacking occur in the opposite of what would be expected if this were the cause of the mobility-MW relationship. This result does not show that in-plane $\pi$-stacking is not important in P3HT, just that it does not cause the mobility dependence on MW. When MW is held constant, our results show a direct correlation between mobility and in-plane $\pi$-stacking. That correlation breaks down when comparing different MWs. These observations suggest that the mobility difference is due to the earlier described domain boundary model, or to effects of the chain length on the electronic properties of the film. The chain length effects could be due to either effects of increased charge transport along the chain or the effect of the longer chains on delocalization of charge carriers between neighboring molecules. Previous work has shown that the longer chains present in polymers reduce the amount of ordering required to obtain strong charge carrier delocalization and band-like conduction compared to that required in small molecule films.[34]

Neher et al have claimed that the low mobility in the low MW films is due to the molecules forming a twisted, disordered structure resulting in crystalline islands in an amorphous matrix.[20] Table 1 and figure 5 show a pronounced shift in the alkyl chain spacing with MW and a slight shift in the in-plane $\pi$-stacking distance. The shift in alkyl chain spacing with MW agrees with that observed by Neher et al[20] and is likely due to a change in the amount of inter-digitation or the tilt angle of the molecules. The observed shift in the in-plane $\pi$-stacking distance is less than 1% and is not expected to have a significant effect on the transport properties. A conformation with the molecules twisting along the chain axis would hinder $\pi$-stacking, and would be expected to increase the $\pi$-stacking distance and broaden the peak due to local variations in the spacing. The observed shift in the $\pi$-stacking is much less than what would be expected for significant

Table 1 – Comparison of the d-spacing and diffraction peak width of each sample.

| Sample | a (Å) $\parallel$ | FWHM (Å$^{-1}$) | a (Å) $\perp$ | FWHM (Å$^{-1}$) | b (Å) | FWHM (Å$^{-1}$) |
|---|---|---|---|---|---|---|
| Low MW | 15.7 | 0.023 | 15.8 | 0.040 | 3.85 | 0.021 |
| High MW | 17.0 | 0.080 | − | − | − | − |
| Low MW Anneal | 15.7 | 0.012 | 15.7 | 0.021 | 3.85 | 0.018 |
| High MW Anneal | 17.0 | 0.039 | − | − | − | − |
| Low MW Xylene | 15.7 | 0.019 | 15.7 | 0.027 | 3.87 | 0.031 |
| High MW Xylene | − | − | 17.0 | 0.060 | 3.81 | 0.065 |
| Low MW Drop cast | 15.7 | 0.010 | 15.8 | 0.026 | 3.87 | 0.017 |
| High MW Drop cast | 16.5 | 0.080 | − | − | 3.82 | 0.075 |

**a** (100) is shown both in-plane ($\parallel$) and out-of-plane ($\perp$). **b** (010) is only shown in-plane.

chain twisting, furthermore the low MW diffraction peaks are much sharper than the high MW ones.

The out-of-plane XRD and AFM of the low MW xylene film show a film with highly ordered domains that does not suggest large amounts of disorder in the bulk of the film. As mentioned in the experimental section, AFM images of the low-MW films are very sensitive to the tip used. Once a tip becomes too dull to resolve the nanorods, the resulting image appears to show partially crystallized films with disordered areas surrounding a web-like network of crystals. This is an imaging artifact that is not representative of the film surface. The AFM data in figure 2 clearly resolves the nanorods in both the topography and the phase images.

Domain boundaries in the low-MW films are either void space or disordered regions due to the steric limitations of the long, rigid polymer chains. A study of the grain boundary limited transport in sexithiophene predicted that charge transport should be thermally activated near room temperature and become independent of temperature at very low temperatures (<80 K).[35]
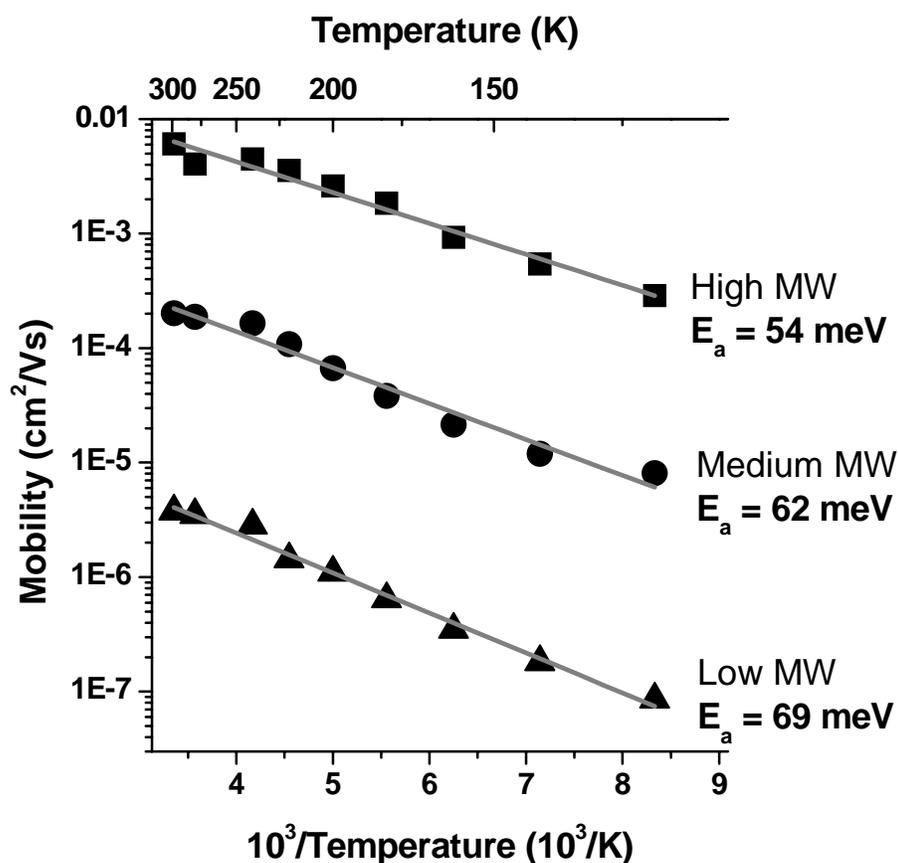
**Figure 7-** Mobility versus temperature for 3 different MW films cast from THF and the calculated activation energy ($E_a$).

Recent results showing that the mobility in P3HT is not thermally activated above room temperature have been used to cast doubt on the grain boundary limiting model.[20] Figure 7 shows that the mobility for each MW is thermally activated below room temperature and that the mobility-MW relationship increases at lower temperature. The mobility starts to decrease above room temperature because the polymer morphology changes. No information about activated charge transport can be obtained in this temperature region because the morphology is not constant. Therefore these results do not conflict with a grain boundary limited model.

Absorption spectra are shown in figure 8. We observe the same blue-shift of the absorption spectrum of low-MW films as reported by Neher et al. [20] The blue-shift of the absorption is the primary evidence for their model of the low-MW molecules forming a twisted, disordered structure that decreases the conjugation length. We believe the blue-shift instead comes from finite size confinement effects of the small molecules. Wohlgenannt et al. have used photoinduced absorption spectroscopy on oligophenylene, oligophenylene-vinylene, oligothiophene (OT) and oligothienylene-vinylene films to show that the absorption due to polarons shifts to lower energy with increasing oligomer length at lengths as large as 7 nm (OT molecules with 17 units).[36] They did not study larger oligomers and therefore did not determine the chain length at which the conjugation length stops increasing and the energy gap saturates. Since a shift in conjugation length is observed in four different molecular structures, and is related to the length of the molecules and not the number of units, it seems unlikely to be explainable by twisting of the chain units. Instead, confinement effects seem most likely.
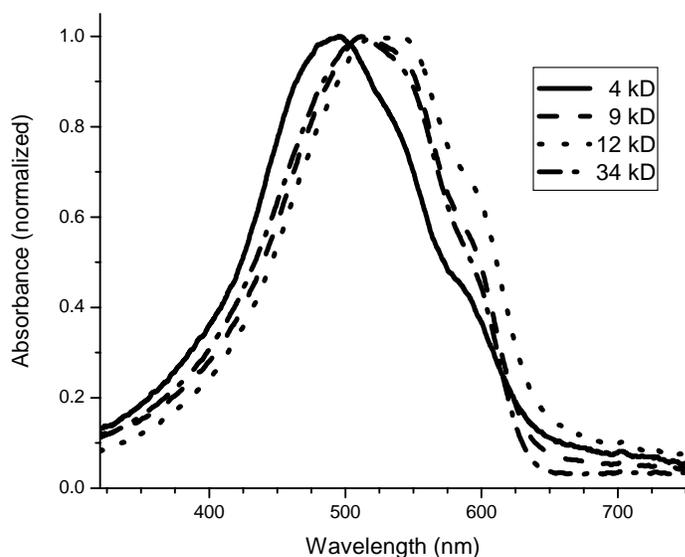


**Figure 8 –** Absorption spectra for various MW films spin-cast from chloroform.

Another reason not to attribute the dependence of mobility on MW to variations in the amount of chain twisting is that medium and high-MW films have similar absorption spectra, despite having different charge carrier mobilities.

**Conclusion**

The dependence of mobility in P3HT on MW has been shown to persist after substantial morphological modifications of the film. Low-MW films are much more sensitive to processing conditions, and their mobilities can be modified by a factor of 100. AFM data shows that using processing conditions that give the chains more time to find an equilibrium position produces films with ordering of the nanorod structure and higher mobility. The overlap between neighboring nanorods is also apparently increased. This observation shows that at least part of the mobility difference between low and high MW is due to morphology and not to the chain length. In-plane GIXS measurements show that when MW is held fixed, the in-plane π-stacking intensity is directly related to changes in mobility. This relationship breaks down when comparing films of different MW. Thus, the amount of in-plane π-stacking is not the primary cause of the dependence of mobility on MW. Instead, we believe the domain boundary structure of the low-MW films or inherent effects of chain length on electronic properties cause the remaining mobility dependence.

**Acknowledgements**

**References**

(1)     Heeger, A. *Angew. Chem. Int. Ed.* **2001**, *40*, 2591-2611.

(2)     Friend, R.;  Gymer, R.;  Holmes, A.;  Burroughes, J.;  Marks, R.;  Taliani, C.;  Bradley, D.;  Dos Santos, D.;  Bredas, J.;  Logdlund, M.; Salaneck, W. *Nature* **1999**, *397*, 121-128.

(3)     Brabec, C.;  Sariciftci, N.; Hummelen, J. *Adv. Funct. Mater.* **2001**, *11*, 15-26.

(4)     Huynh, W. U.;  Dittmer, J. J.; Alivisatos, A. P. *Science* **2002**, *295*, 2425-2427.

(5)     Coakley, K. M.; McGehee, M. D. *Chem. Mater.* **2004**, *16*, 4533-4542.

(6)     Dimitrakopoulos, C.; Malenfant, P. *Adv. Mater.* **2002**, *14*, 99.

(7)     Katz, H.; Bao, Z. *J. Phys. Chem. B* **2000**, *104*, 671-678.

(8)     Horowitz, G. *J. Mater. Res.* **2004**, *19*, 1946-1962.

(9)     Salleo, A.;  Chabinyc, M.;  Yang, M.; Street, R. *Appl. Phys. Lett.* **2002**, *81*, 4383-4385.

(10)    Sirringhaus, H.;  Wilson, R.;  Friend, R.;  Inbasekaran, M.;  Wu, W.;  Woo, E.;  Grell, M.;  Bradley, D. *Appl. Phys. Lett.* **2000**, *77*, 406-408.

(11)    Chabinyc, M. L.;  Lu, J.-P.;  Street, R. A.;  Wu, Y.;  Liu, P.; Ong, B. S. *J. Appl. Phys.* **2004**, *96*, 2063-2070.

(12)    Ong, B. S.;  Wu, Y. L.;  Liu, P.; Gardner, S. *J. Am. Chem. S.* **2004**, *126*, 3378-3379.

(13)    Bao, Z.;  Dodabalapur, A.; Lovinger, A. *Appl. Phys. Lett.* **1996**, *69*, 4108-4110.

(14)    Sirringhaus, H.;  Tessler, N.; Friend, R. H. *Science* **1998**, *280*, 1741.

(15)    Raja, M.;  Lloyd, G.;  Sedghi, N.;  Eccleston, W.;  Di Lucrezia, R.; Higgins, S. *J. Appl. Phys.* **2002**, *92*, 1441-1445.

(16)    Wang, G.;  Swenson, J.;  Moses, D.; Heeger, A. J. *J. of Appl. Phys.* **2003**, *93*, 6137-6141.

(17)    Babel, A.; Jenekhe, S. *J. Phys. Chem. B* **2003**, *107*, 1749-1754.

(18)   Sirringhaus, H.;  Brown, P. J.;  Friend, R. H.;  Nielsen, M. M.;  Bechgaard, K.;
       Langeveld-Voss, B. M. W.;  Spiering, A. J. H.;  Janssen, R. A. J.;  Meijer, E. W.;
       Herwig, P.; de Leeuw, D. M. *Nature* **1999**, *401*, 685-688.

(19)   Kline, R. J.;  McGehee, M. D.;  Kadnikova, E. N.;  Liu, J.; Frechet, J. M. J. *Adv. Mater.*
       **2003**, *15*, 1519-1522.

(20)   Zen, A.;  Pflaum, J.;  Hirschmann, S.;  Zhuang, W.;  Jaiser, F.;  Asawapirom, U.;  Rabe,
       J. P.;  Scherf, U.; Neher, D. *Adv. Funct. Mater.* **2004**, *14*.

(21)   Chang, J.-F.;  Sun, B.;  Breiby, D. W.;  Nielson, M. M.;  Solling, T. I.;  Giles, M.;
       McCulloch, I.; Sirringhaus, H. *Chem. of Mater.* **2004**, *NA*.

(22)   Tanase, C.;  Meijer, E. J.;  Blom, P. W. M.; de Leeuw, D. M. *Phys. Rev. Lett.* **2003**, *91*,
       216601.

(23)   Knaapila, M.;  Kisko, K.;  Lyons, B. P.;  Stepanyan, R.;  Foreman, J. P.;  Seeck, O. H.;
       Vainio, U.;  Palsson, L. O.;  Serimaa, R.;  Torkkeli, M.; Monkman, A. P. *J. Phys. Chem.
       B* **2004**, *108*, 10711-10720.

(24)   Banach, M.;  Friend, R.; Sirringhaus, H. *Macromolecules* **2003**, *36*, 2838-2844.

(25)   Goh, C.;  Kline, R. J.;  McGehee, M. D.;  Kadnikova, E. N.; Frechet, J. M. J. *Polymer
       Preprints* **2004**, *45*, 210-211.

(26)   Salaneck, W. R.;  Inganas, O.;  Themans, B.;  Nilsson, J. O.;  Sjogren, B.;  Osterholm, J.-
       E.;  Bredas, J.-L.; Svensson, S. *J. Chem. Phys.* **1988**, *89*, 4613-4619.

(27)   Schwartz, B. J. *Annual Review of Physical Chemistry* **2003**, *54*, 141-172.

(28)   Liu, J. S.;  Sheina, E.;  Kowalewski, T.; McCullough, R. D. *Angew. Chem. Int. Ed.* **2001**,
       *41*, 329-+.

(29)   Horowitz, G. *Adv. Mater.* **1998**, *10*, 365-377.

(30)    Sandberg, H.;  Frey, G.;  Shkunov, M.;  Sirringhaus, H.;  Friend, R.;  Nielsen, M.;

Kumpf, C. *Langmuir* **2002**, *18*, 10176-10182.

(31)    Breiby, D. W.; Samuelsen, E. J. *J. Polym. Sci. Pt. B-Polym. Phys.* **2003**, *41*, 2375-2393.

(32)    Prosa, T.;  Moulton, J.;  Heeger, A.; Winokur, M. *Macromolecules* **1999**, *32*, 4000-4009.

(33)    Heffner, G. W.; Pearson, D. S. *Macromolecules* **1991**, *24*, 6295-6299.

(34)    Beljonne, D.;  Cornil, J.;  Sirringhaus, H.;  Brown, P.;  Shkunov, M.;  Friend, R.; Bredas,

J. *Adv. Funct. Mater.* **2001**, *11*, 229-234.

(35)    Horowitz, G. *Adv. Funct. Mater.* **2003**, *13*, 53-60.

(36)    Wohlgenannt, M.;  Jiang, X.;  Vardeny, Z.; Janssen, R. *Phys. Rev. Lett.* **2002**, *88*,

197401-197401.